Chemical Engineering Journal 160 (2010) 351–362

Contents lists available at ScienceDirect

Chemical Engineering Journal

journal homepage: www.elsevier.com/locate/cej

Experimental and theoretical investigations of the coating of capsules with titanium dioxide

Martin Sgraja[a,*], Jan Blömer[a], Jürgen Bertling[a], Peter J. Jansens[b]

[a] Fraunhofer Institute for Environmental, Safety, and Energy Technology UMSICHT, Business Unit Advanced Materials, Osterfelder Strasse 3, 46047 Oberhausen, Germany
[b] Delft University of Technology, Dept. Process & Energy Laboratory, Leeghwaterstraat 44, 2628 Delft, The Netherlands

ARTICLE INFO

Article history:
Received 22 June 2009
Received in revised form 12 February 2010
Accepted 26 February 2010

Keywords:
Thermal hydrolysis
Titanium dioxide
Precipitation
Coating
Population balance equation

ABSTRACT

Titanium dioxide is a ceramic material which is widely used as a white pigment and catalyst. In the present work the precipitation of TiO_2 by the thermal hydrolysis of titanium oxysulphate was studied in terms of the homogeneous precipitation and the coating of capsules. Experimental work and simulations have been done to describe the precipitation in 0.1 M aqueous solutions while in some experiments sulphuric acid was added to increase the reaction time. In the experimental part of this work, gravimetric and spectroscopic measurements were performed to determine the time-dependent precipitation of the material and particle size measurements to characterize the time-dependent size distribution of the precipitated particles. In the theoretical part different mechanisms of the precipitation process like nucleation, growth and agglomeration were considered using semi-empirical equations. For the transfer of the effects of the individual particle scale to the whole population of particles population balance equations (PBEs), one for the colloidal and one for the deposited phase, were used. Finally, the theoretical results were compared to the experimental ones and the limitations of the model were discussed.

1. Introduction

Titanium dioxide is a ceramic material which is widely used as a white pigment and catalyst. The process which is mainly used for its production is the sulphate process. In this process naturally occurring ilmenite ($FeTiO_3$) is reduced to titanium slag at 1200 °C and treated with concentrated sulphuric acid and scrap metal to reduce Fe^{3+} to Fe^{2+} which would otherwise lead to impurities of precipitated $Fe(OH)_3$. By a subsequent treatment with water at temperatures below 85 °C the titanium dissolves in form of $TiOSO_4$ and, after removal of $FeSO_4{\cdot}7H_2O$ by cooling crystallization, titanium oxysulphate can be hydrolyzed to titanium oxide at elevated temperatures [1]. For the set-up of the properties of the final product the process in which the hydrolyzation step is the most essential part has to be carefully controlled. In this step the titanyl sulphate reacts with water to form titanium oxyhydrate and sulphuric acid while the rate of hydrolysis depends on the temperature and the concentration of $TiOSO_4$ and H_2SO_4. It increases, with decreasing concentration of $TiOSO_4$ and H_2SO_4, due to the shift of the equilibrium to the side of the products, and with increasing temperature due to the positive activation energy [e.g. 2]. After the hydrolyzation the titanium oxide hydrate forms oxo (olation) and hydroxo (oxilation) bridges while oxo bridges are favored by higher temperatures [3]. In this condensation process gel particles are formed which on the other hand can dissolve again. After reaching a certain size, which depends on the interfacial tension between the particles and the solution, the particles are stable and referred to as critical nuclei. Thus, the nucleation rate can either be increased by decreasing concentrations of $TiOSO_4$ leading to an increased hydrolyzation rate or by the addition of seeds (e.g. mica [4,5]) which provide sites of reduced interfacial tension and reduce the critical size of the nuclei [5]. After nucleation the particles can either increase their size by further condensation of monomeric building blocks at the surface, which is referred to as growth, or by collision and formation of solid connections to other particles which is referred to as agglomeration. In case of high concentrations of $TiOSO_4$ and thus low nucleation rates the amount of the precipitated TiO_2 strongly depends on the number of seeds [4] which also means that the main part of the material is precipitated by growth. In the agglomeration process Sathyamoorthy et al. [6–8] differentiated between aggregation and agglomeration. He found that aggregates, clusters of particles, with strong chemical bonds or crystal bridges, were formed at high supersaturations by secondary nucleation at the surfaces of small nuclei. Agglomerates on the other hand were formed at low supersaturations while the particles were mainly bound by weak bonds where SO_4^{2-} bridges play a major role. Since he found

* Corresponding author. Present address: Heerstrasse 25, 52441 Linnich, Germany. Tel.: +49 170 4845948.
E-mail addresses: sgraja@muenster.de (M. Sgraja), jan.bloemer@umsicht.fraunhofer.de (J. Blömer), juergen.bertling@umsicht.fraunhofer.de (J. Bertling), p.j.jansens@tudelft.nl (P.J. Jansens).

1385-8947/$ – see front matter © 2010 Elsevier B.V. All rights reserved.
doi:10.1016/j.cej.2010.02.061

Nomenclature

Symbols

A	specific surface ($m^2\ g^{-1}$)
B	nucleation, birth rate ($m^{-3}\ s^{-1}$)
c	concentration ($mol\ L^{-1}$)
C_c	molar density of crystals ($mol\ m^{-3}$)
d	stirrer diameter (m)
$d_{4,3}$	volume weighted mean diameter (m)
D	death rate ($m^{-3}\ s^{-1}$)
D_{AB}	diffusion coefficient ($m^2\ s^{-1}$)
g	growth rate exponent
G	growth rate ($m\ s^{-1}$)
I_s	degree of segregation
k_B	Boltzmann constant ($kg\ m^2\ s^{-2}\ K^{-1}$)
$k_1 = k_g$	growth rate constant ($m\ s^{-1}$)
k_2	pre-exponential nucleation constant (m^{-3})
k_3	nucleation constant
k_c	trapping constant (s^{-1})
k_r	surface integration constant ($kg\ m^{-2}\ s^{-1}$)
k_{r1}	first chemical reaction constant ($mol\ L^{-1}\ s^{-1}$)
k_{r2}	second chemical reaction constant ($mol\ L^{-1}\ s^{-1}$)
K	instrument constant XRD, Eq. (23)
L_0	initial size of the nuclei (m)
L_j, L_k	size of particle j and k (m)
m	mass (kg)
$\dot{m}$	mass flux ($kg\ m^{-2}\ s^{-1}$)
n	stirring rate (s^{-1})
$n(L)$	number density (m^{-4})
N_A	Avogadro constant (mol^{-1})
N_j, N_k	number of particles j and k
r_{agg}	agglomeration rate (s^{-1})
r_{coll}	collision rate (s^{-1})
R	gas constant ($kg\ m^2\ s^{-2}\ K\ mol$)
Re	Reynolds number
S	supersaturation
Sc	Schmidt number
t	time (s)
T	absolute temperature (K)
V_R	volume of the reaction solution (m^3)

Greek symbols

β	agglomeration kernel (s^{-1})
β	full with at half height, Eq. (23)
γ_{CL}	interfacial tension between the crystal and the liquid ($N\ m$)
$\dot{\gamma}$	shear rate (s^{-1})
Δc	change of concentration ($mol\ L^{-1}$)
ε	specific power input ($W\ kg^{-1}$)
θ	mixing time (s)
θ	angle of X-ray reflex Eq. (23) (°)
λ	Kolmogorov microscale (m)
μ	dynamic viscosity (Pa s)
ν	kinematic viscosity ($m^2\ s^{-1}$)
ν_{+-}	number of positive and negative ions
ρ	density ($kg\ m^{-3}$)
τ_{edd}	lifetime of eddies (s)
τ_D	characteristic mixing time (s)
ψ_{eff}	collision efficiency

Subscripts

agg	agglomeration
app	appearing
br	Brownian
c	colloidal phase
d	deposited phase
diss	disappearing
equil	equilibrium
hom	homogeneous
L	liquid
macro	macro-mixing
micro	micro-mixing
nuc	nucleation
p	particle
reac	reaction
tr	turbulent

that the aggregate size was dependent on the stirrer speed and the size of the particles were smaller than the Kolmogorov microscale he deduced that the aggregation mechanism was mainly based on an orthokinetic mechanism [7]. The agglomerate size depended on the stirrer speed, too, but decreased with increasing energy input showing a prevailing perikinetic mechanism. Thus, the precipitation of titanium dioxide as a solid material covers the four steps hydrolyzation, nucleation, growth and agglomeration. Naturally, these steps are not independent but occur at the same time.

Beneath the homogeneous precipitation of the material the sulphate process can also be used for the coating of polymeric particles and capsules. This is for example used in electronic ink displays to combine the good optical properties of the oxide with the low density of the polymeric core [9] and in the formation of inorganic and organic–inorganic hollow spheres. In the latter microcapsules, liquid filled particles, are coated with TiO_2 before in a subsequent step the capsule or the liquid from within the capsule is removed by dissolution or burning out leaving back a gas filled hollow sphere [10,11]. Due to the gas filled cavity and thus the low density such hollow spheres are most frequently used as fillers for polymers and ceramics to reduce the weight of the materials. This leads to cost reduction by the saved material as well by reduced transport costs [12].

In literature a number of publications can be found dealing with the thermal hydrolysis of titanium oxy sulphate either covering the homogeneous precipitation [e.g. 2,13,14] or the coating of particles [4,15], fibres [16] and flat surfaces [17,18]. However, there is only little information about the coating of organic particles by this process. Thus, in the present work the precipitation mechanism of titanium dioxide with and without such capsules was investigated. For this purpose the time-dependent precipitation in water and diluted sulphuric acid was measured by gravimetric analysis and UV/vis spectroscopy and the primary particle size as well as the agglomerate size was determined. For the characterization of the coating, the time-dependent precipitation on the capsules was measured in the presence of capsules with a total surface of 4 and $20\ m^2\ L^{-1}$.

Additionally, further results were derived from a model covering simple equations for nucleation, growth and agglomeration and a population balance equation for particle size density distributions of the particles in solution and precipitated on the capsules.

2. Theory

2.1. Dosing and mixing

For extraction of suitable data, e.g. particle diameters or precipitated masses from experiments, it is of crucial importance that the mixing is faster than the reaction of the components. In this way concentration gradients and thus different starting conditions

within the vessel are prevented. Under turbulent conditions the mixing process can be described by the turbulence theory of Kolmogorov [19]. It is assumed that the energy from the stirrer is initially transformed into large eddies. The energy of these eddies is subsequently transferred by shearing and stretching into smaller eddies until in the smallest units the viscous forces dominate and all the energy is dissipated into heat. In his work Kolmogorov assumes that after a sufficient number of steps in this so-called energy cascade local isotropic turbulence prevails. A sufficient number of steps is met when the Reynolds number $Re = nd^2 \rho_L \mu^{-1} > 1 \times 10^4$. Here n is the stirring rate, d the diameter of the stirrer, ρ the density and μ the viscosity of the liquid. Kolmogorov additionally derived that the size of the smallest eddies λ only depends on the specific energy input ε and the kinematic viscosity ν.

$$\lambda = \left(\frac{\nu^3}{\varepsilon}\right)^{1/4} \tag{1}$$

The size of the smallest eddies is defined as the microscale of mixing or as Kolmogorov microscale. Analogously a range of turbulence at the macroscale is defined, which is approximately the size of the stirrer diameter.

To assess the macro- and micro-mixing time Geisler et al. [20] defined a time-dependent degree of segregation $I_s = \exp(-t/\tau_D)$, where t is the time and τ_D a characteristic time, which describes the extent of mixing between 1 completely separated ($t = 0$) and 0 completely mixed ($t \to \infty$). The macro-time of mixing for a degree of segregation of about 0.01–0.05 can then be assessed by Eq. (2) [21] and the micro-mixing time in dependence of the degree of segregation for a Schmidt number $Sc > 100$ ($Sc = \nu/D_{AB}$) by Eq. (3) [20]. The Schmidt number gives the ratio between the kinematic viscosity and the diffusion coefficient D_{AB}.

$$\theta_{macro} \approx 7.3\left(\frac{d^2}{\varepsilon}\right)^{1/3} \tag{2}$$

$$\theta_{micro} = \frac{0.5(\nu/\varepsilon)^{1/2}(0.88 + \ln Sc)(1 - I_s)}{I_s} \tag{3}$$

After measuring the macro-mixing time, Eq. (2) can be used to assess the specific energy input which is subsequently used to calculate the micro-mixing time and the Kolmogorov microscale. The Kolmogorov microscale can later be used again to determine the mechanism of agglomeration for the modeling of the precipitation process.

2.2. Chemical kinetics

For the evaluation of the chemical kinetics the data given by Duncan and Richards [22] were used. They investigated the thermal hydrolysis of $TiOSO_4$ by measuring the degree of hydrolyzation using UV/vis spectroscopy. They found that the absorbance-time curves for the charge transfer of $Ti(OH)_3^+$ measured at 225 nm show the typical characteristics of a chemical reaction containing an intermediate species. Together with the data of Beukenkamp and Herrington [23] they derived the following mechanism for the thermal hydrolysis of $TiOSO_4$.

$$Ti(OH)_3HSO_4\ (aq.) \xrightarrow{kr1} Ti(OH)_3{}^+\ (aq.) \xrightarrow{kr2} TiO_2 \cdot H_2O\ (s) \tag{4}$$

Following these equilibria they found that the initial reaction rate k_{r1} is inversely proportional to the total HSO_4^- concentration yielding $k_{r1} = k'_{r1} c(HSO_4^-)^{-1}$ with $k'_{r1} = 9.3 \times 10^{-5}$ mol L^{-1} s^{-1}. For the second reaction rate a value of $k_{r2} = 1.1 \times 10^{-4}$ mol L^{-1} s^{-1} is given. Since these values were obtained at room temperature while the present investigations were done at 80 °C the parameters had to be extrapolated to the higher temperature. For this purpose the temperature-dependent data of the reaction constants given in the article have been used giving the following Arrhenius equations.

$$k_{r1} = 6.68 \times 10^{14}\ \text{mol L}^{-1}\ \text{s}^{-1} \exp\left(\frac{-105.7\ \text{kJ mol}^{-1}}{RT}\right); \tag{5}$$

$$k_{r2} = 9.28 \times 10^{13}\ \text{mol L}^{-1}\ \text{s}^{-1} \exp\left(\frac{-100.5\ \text{kJ mol}^{-1}}{RT}\right) \tag{5a}$$

2.3. Modeling

As described above the precipitation of a saturated solution can be divided into hydrolyzation, nucleation, growth, and agglomeration. In case of the nucleation, primary homogeneous and heterogeneous and secondary nucleation mechanisms are known. As will be shown later, in the present system very high supersaturations are established so that it is assumed that only primary, homogeneous nucleation has to be considered. One way to describe the nucleation process is the classical theory of nucleation [24]. In this theory it is assumed that by the collision of molecules small particles, so-called clusters, are formed which are unstable before reaching a critical size. Once the critical size is exceeded the particles are referred to as nuclei. Beyond this critical size the free enthalpy of formation decreases with increasing size and the nuclei are continuously growing. Considering the free volume and surface enthalpy as well as the interfacial tension γ_{CL} between the nuclei and the supersaturated solution an equation for the homogeneous nucleation B_{hom} in solution can be derived [24].

$$B_{hom} = 1.5 D_{AB} (C_c N_A)^{7/3} \sqrt{\frac{\gamma_{CL}}{kT}} \frac{1}{C_c N_A} \times \exp\left[-\frac{16}{3}\pi \left(\frac{\gamma_{CL}}{kT}\right)^3 \left(\frac{1}{C_c N_A}\right)^2 \frac{1}{\nu_{+-}^2\ \ln^2 S}\right] \tag{6}$$

Here D_{AB} is the diffusion coefficient, C_c the molar density, N_A the Avogadro constant, ν_{+-} the number of ions and S the supersaturation ratio. The supersaturation which is the driving force of the nucleation is defined as $S = c/c_{equil}$ with c the actual and c_{equil} the equilibrium concentration. Since the determination of the variables, especially the interfacial tension between the particles and the surrounding solution, is quite difficult in this work an empirical approach Eq. (7) is used [25].

$$B_{hom} = k_2\ \exp\left(\frac{-k_3}{\ln^2 S}\right) \tag{7}$$

For the development of Eq. (7) the supersaturation was defined by concentrations which is a simplification that only holds for well soluble salts where the activity coefficients of the solute and the equilibrium state are the same. Thus, for sparingly soluble salts the activity based supersaturation, taking into account the ionic strength and the valences of the ions, should be used. In literature there are only theories describing the activities at low ionic strengths (e.g. Güntelberg or Davies equation [26]) or they require a number of thermodynamic data which are not available for titanium oxysulphate at 80 °C. However, when the reaction between $TiOSO_4$ and water is of the form

$$Ti(OH)_3{}^+ + HSO_4{}^- + H_2O \rightarrow TiO(OH)_2 + H^+ + HSO_4{}^- \tag{8}$$

assuming that the dominant species are $Ti(OH)_3{}^+$ and $HSO_4{}^-$, which is supported by the results of Beukenkamp and Herrington [23], then the consumption of one $Ti(OH)_3{}^+$ will lead to the formation of one H^+. Consequently, the ionic strength during the hydrolysis is constant and the activity coefficients for the species in solution and in the equilibrium state can be assumed to be the same and can thus be omitted.

The second mechanism which has to be considered is growth with the growth rate G which can be defined as a mean growth rate for all particles derived from the overall mass flux density [24]. If it is assumed that the system is ideally mixed and that the growth is governed by the surface integration step then the mass flux is directly proportional to the concentration difference and the growth rate can be expressed using the density of the precipitated material.

$$\dot{m} = k_r \Delta c^g; \quad G = \frac{\dot{m}}{\rho} = \frac{k_r \Delta c^g}{\rho} = k_g \Delta c^g \quad \text{with} \quad \Delta c = c - c_{equil} \tag{9}$$

Here k_r is the surface rate integration constant, k_g the growth rate constant and g the growth rate exponent. At high supersaturations the concentration gradient can be expressed as $\ln S$ so that the following expression for the growth rate is yield.

$$G = k_g (\ln S)^g \tag{10}$$

For the description of the agglomeration process the collision of particles and their adhesion to each other has to be considered. The first is described by a collision rate r_{coll} while the second part is described by a collision efficiency ψ_{eff} [27]. For the description of the collision rate ($r_{coll} = \beta_0 \cdot \beta(L_1, L_2)$) a size dependent $\beta(L_j, L_k)$ and a size independent agglomeration kernel β_0 are used. In this way the agglomeration rate can be described as

$$r_{agg} = \psi_{eff} \cdot r_{coll} \cdot N_j \cdot N_k = \psi_{eff} \cdot \beta_0 \cdot \beta(L_j, L_k) \cdot N_j \cdot N_k \tag{11}$$

where N_j and N_k are the number of particles of size j and k, respectively [27]. For the description of the agglomeration process the kernels for Brownian motion (perikinetic) (12) and turbulence (orthokinetic) Eq. (13) agglomeration developed by Smoluchowski were used [28]. The perikinetic kernel describes the agglomeration of particles smaller than the Kolmogorov microscale whereas the orthokinetic kernel is used for larger particles which are affected by the fluid shear.

$$\beta_{br} = \frac{2kT}{3\mu}(L_j + L_k)\left(\frac{1}{L_j} + \frac{1}{L_k}\right) \tag{12}$$

$$\beta_{tur} = \frac{4}{3}\dot{\gamma} \cdot \left(\frac{L_j}{2} + \frac{L_k}{2}\right)^3 = \frac{1}{6}\dot{\gamma} \cdot (L_j + L_k)^3 \tag{13}$$

The amount of shear rate $\dot{\gamma}$ is inversely proportional to the life time of the eddies which again depends on the specific power input and the kinematic viscosity of the solution.

$$\dot{\gamma} = \frac{1}{\tau_{edd}} \tag{14}$$

$$\tau_{edd} = \sqrt{\frac{\nu}{\varepsilon}} \Rightarrow \dot{\gamma} = \sqrt{\frac{\varepsilon}{\nu}} \tag{15}$$

In the present work both mechanisms were incorporated into the model to describe the agglomeration process. For the description of the agglomeration efficiency the model developed by Hounslow et al. was used [27]. The dependence on agglomeration from supersaturation in this work was taken into account by direct coupling of the agglomeration term with the supersaturation while other static parameters were combined with the agglomeration constants (β_{br}, β_{tr}) to yield the following equation:

$$r_{agg} = S\beta_{br}(L_j + L_k)\left(\frac{1}{L_j} + \frac{1}{L_k}\right) + S\beta_{tr}(L_j + L_k)^3. \tag{16}$$

2.4. Population balance equation (PBE)

To link the effects of the individual particle scale to the whole population of particles population balance equations were chosen [29]. The formulation of a PBE is based on the number density distribution $n(L)$ which is the number of particles per unit volume and size class. A PBE describes the particle distribution function with respect to all processes that generate, resize or remove particles from the distribution. For this purpose a set of external and internal coordinates are defined where the external coordinates represent the spatial position within the system and the internal coordinates represent the properties like size, volume and surface area of the particles. In the present work a population balance equation for the colloidal particles in solution and for the particles deposited on the cores was formulated. In both cases the size L of the particles was taken as the internal coordinate. The PBE for the colloidal phase is [30]:

$$\frac{\partial n_c(L)}{\partial t} + G_c \frac{\partial n_c(L)}{\partial L} = +\delta(L - L_0)B_{nuc} + B_c(L)_{agg} - D_c(L)_{agg} - D_c(L)_{dis} \tag{17}$$

The first term on the left hand side $n_c(L)$ accounts for the change of the number density of the particles of size range L and the second term for the growth of the particle in which it is assumed that the growth rate in the colloidal phase G_c is independent of the particle size, i.e. there is no growth rate dispersion. On the right hand side the first two terms account for the formation of particles due to nucleation and agglomeration while the third and fourth term represent the disappearance of particles due to agglomeration and trapping on the cores, respectively. For the nucleation it is assumed that new particles are quite small and thus only formed in the first size class L_0. If B is taken as the nucleation rate of primary particles of infinitesimal small size then $B_{hom} = B/dL_1$. The disappearance of particles by trapping can be described by a trapping constant k_c, the specific surface area A_{cores}, the mass of the cores m_{cores} as well as the volume of the reaction solution V_R.

$$D_c(L)_{dis} = k_c \frac{A_{cores} m_{cores}}{V_R} n_c(L) \tag{18}$$

The PBE for the deposited phase can be formulated in the same way taking $n_d(L)$ as the number density distribution of the trapped particles:

$$\frac{\partial n_d(L)}{\partial t} + G_d \frac{\partial n_d(L)}{\partial t} = B_d(L)_{app} \tag{19}$$

In this case G_d is the growth rate of the particles within the coating layer and $B_d(L)_{app}$ the term for the trapping of colloidal particles on the cores with $B_d(L)_{app} = D_c(L)_{dis}$.

Additionally, a mass balance was used for the colloidal phase where in addition to nucleation and growth and trapping of the particles the chemical reaction is taken into account [30].

$$\frac{dc}{dt} = \left(\frac{dc}{dt}\right)_{reac} + \left(\frac{dc}{dt}\right)_{nucl} + \left(\frac{dc}{dt}\right)_{growth} + \left(\frac{dc}{dt}\right)_{coating} \tag{20}$$

As described above Eq. (4) the chemical reaction from titanium oxysulphate to titanium oxide proceeds via an intermediate. In this way the concentration of the product c_{TiO_2} can be calculated as [31]

$$c_{TiO_2} = c_{0,TiOSO_4}\left[1 + \frac{k_{r1}\exp(k_{r2}t) - k_{r2}\exp(-k_{r1}t)}{k_{r2} - k_{r1}}\right]. \tag{21}$$

For the solution of the equation only the two reaction constants k_{r1} and k_{r2} and the initial concentration of the $TiOSO_4$ solution $c_{0,TiOSO_4}$ are needed.

For the solution of the PBE and the mass balance a simulation program developed by Zafar was applied [30]. Solving of the PBEs was done using a discretization approach based on the finite volume method described by Lim et al. [32]. In the discretized growth term the numerical fluxes were calculated according to the high resolution numerical scheme called WENO [33], in addition for a high resolution near steep ends the artificial compression method

(ACM) described by Yang [34] was implemented. For the agglomeration term a discretized approach given by Kumar and Ramkrishna [35] was taken.

3. Experimental

3.1. Materials and methods

Titanium(IV) oxysulphate was purchased from Sigma–Aldrich (Seelze, Germany). 0.1 M H_2SO_4 was prepared by dilution of concentrated sulphuric acid purchased from Sigma–Aldrich (Seelze, Germany). Separation of the precipitates from solutions was either done using a polypropylene (PP) membrane Accurel PP 2E HF R/P (Membrana, Germany) with a nominal pore size of 0.2 μm or by syringe filters Rotilabo CME (Carl Roth GmbH, Germany) with a pore size of 0.22 μm. For the determination of the titanium concentration by UV/vis-spectroscopy hydrogen peroxide (Perhydrol, pro analysi, Merck, Darmstadt) was used. For the coating process polyamine microcapsules with a liquid core of tetradecane were used. The capsules were synthesized using an in situ polymerization of melamine-formaldehyde precondensates [10,11]. The size distribution of the capsules was typically bimodal with a volume and surface weighted mean particle size of $d_{4,3}$ = 19.7 and $d_{3,2}$ = 9.4 μm, respectively. The specific surface was calculated to be 0.8 $m^2\,g^{-1}$ taking into account a capsule density of 0.8 $g\,cm^{-3}$.

3.2. Determination of the solubility of TiO_2

Since it can be expected that the solubility of freshly precipitated titanium dioxide is considerably higher than that of aged material the solubility of titanium dioxide was measured with freshly precipitated material. For this purpose a precipitation according to the standard operation was performed at 80 °C using a 0.1 M solution of $TiOSO_4$. After 6 h of hydrolyzation at 80 °C the precipitate was separated from the solution and extensively washed with distilled water. Small amounts of the oxide were mixed with distilled water and the solutions were adjusted to different pH using diluted sulphuric acid. Afterwards, the solutions were equilibrated at 80 °C in a shaking bath for 1 week. For the analysis of the samples the solutions were filtered through a 0.2 μm membrane while hot and the concentration of titanium was measured using inductive coupled plasma (ICP) spectroscopy (Ultima 2, Fa. Horiba Jobin Yvon, Munich). The solubility of titanium dioxide in dependence of the H^+-concentration was found to be $c(TiO_2)_{aq}$ = 27.2 mg L^{-1} $c(H_3O^+)^{0.8}$.

3.3. Determination of the dosing and mixing time

The dosing time was measured using the color change of an indicator. The vessel was filled with 452 mL hydrochloric acid containing 4.52 mmol HCl. Additionally, bromthymol blue (Merck, Darmstadt) as an indicator, showing a color change from orange to blue at a pH of seven, was added to the vessel. Under stirring at 300 rpm 48 mL of a solution containing 4.56 mmol sodium hydroxide was added by means of a 50 mL syringe pump. The excess of NaOH was used to gain a distinct color change. In the dosing step firstly the time for the dosing and secondly the time to the visually detected point of the color change was stopped. The dosing and mixing time were measured three times and the values averaged.

3.4. Thermal hydrolysis

For the precipitation of the titanium dioxide the titanium(IV) oxysulphate was dissolved in distilled water and the clear solution was filtered through a 0.2 μm polypropylene membrane to remove particles and impurities. In parallel 452 mL of distilled water, including the appropriate amount of sulphuric acid, and in case of the coating experiments the microcapsules, was heated up to 84 °C while stirring at 300 rpm. Reaching a constant temperature 48 mL of the $TiOSO_4$ solution were added under continuous stirring by means of a syringe pump to give a total volume of 500 mL. The mass of the titanium oxysulphate was calculated according to an overall concentration of 0.1 mol L^{-1}. By adding the titanium solution of about room temperature the temperature in the vessel drops to the final working temperature of 80 °C. After distinct time steps samples were taken, quenched in an ice bath to stop the thermal reaction and analyzed with respect to precipitation rate, morphology and primary particle and agglomerate size.

3.5. Gravimetric analysis

For the gravimetric analysis 20 mL samples of the suspension were taken, quenched in an ice bath and filtered through a 0.2 μm PP membrane. The filter cake together with the filter was quantitatively transferred into a weighted porcelain crucible, dried at 105 °C and calcined at 800 °C. Previously it was checked that the polymeric membrane burns residue free. From the remaining mass, which was considered to consist only of TiO_2, the percentage of precipitated titanium dioxide was calculated.

3.6. Spectroscopic determination of titanium

Additionally, the Ti-concentration was determined spectroscopically (408 nm) by measuring the yellow-orange complex formed by the reaction of titanium(IV) with hydrogen peroxide [36,1].

$$[Ti(OH)_2(H_2O)_4]^{2+} + H_2O_2 \rightarrow [Ti(O_2)\cdot aq]^{2+} + 6H_2O \quad (22)$$

$$[Ti(OH)_3]^{+} + H_2O_2 \rightarrow [Ti(O_2)(OH)]^{+} + 2H_2O \quad (22a)$$

Previously a calibration line using $TiOSO_4$ solutions of known concentrations in a concentration range between 2×10^{-5} and 12×10^{-5} mol L^{-1} was measured. For this purpose $TiOSO_4$, where the exact concentration was measured by inductive coupled plasma (ICP) measurements, was dissolved in distilled water and appropriated volumes were transferred to a 50 mL volumetric flask. 0.5 mL H_2O_2 (30 wt.%) was added to the solution and the volumetric flask was filled up with 0.1 M H_2SO_4. Since it was found that the absorption increases with time all the measurements were performed 2 h after adding the hydrogen peroxide. It was found that after this time the absorption was almost constant. The molar absorption coefficient was found to be 688.6 L mol^{-1} cm^{-1}.

For the measurement of the reaction solutions the samples were quenched in an ice bath and filtered through a 0.22 μm syringe filter. The sample preparation was performed analogously to that of the calibration line.

3.7. SEM

For the investigation of the particle morphology scanning electron microscopy (SEM, ESEM Quanta 400, Fei Company) was used. Prior to SEM investigations the samples were coated with a thin conducting layer of a gold/palladium (20%) (Sputter Coater K550, Emitech).

3.8. Primary particle and agglomerate size

For the measurement of the primary particle size X-ray diffraction (XRD) was used while it was assumed that the primary particles correspond to the smallest crystalline areas measured. The advantage of this method is that the primary particle size can be measured disregarding the aggregation of the particles. With this technique

the primary particle size can be derived from the line broadening of the reflexes using the Scherer equation [38].

$$L = \frac{K\lambda}{\beta \cos\theta} \tag{23}$$

Here L is the size of the crystallites, K an instrument constant taken as 0.9, β the full width at half height and θ the angle of the reflex. For the measurement of the samples a powder diffractometer (STOE, Stadi-P) with monochromatic Cu Kα radiation in transmission and for the analysis of the data the software FIT (STOE) was used.

For the determination of the agglomerate size static light scattering (Mastersizer 2000, Hydro 2000 μP, Malvern Instruments) was used. Diluted sulphuric acid (0.1 M) was used as the measurement liquid to prevent further precipitation during the measurement. Analysis of the data was performed using the Mie-theory with a refractive index of (2.493).

4. Results and discussion

4.1. Dosing and mixing

As described above the mixing time was measured to ascertain if the system is ideally mixed. Using a 50 mL syringe pump the dosing time was about 7.4 s and the mixing time including the dosing step about 11.0 s. However, in the experiments it was found that directly after the addition of the titanium oxysulphate solution to the water the solution becomes turbid, whereas when adding the $TiOSO_4$ solution to 0.1 M H_2SO_4 the turbidity was first detected after 2 min. The cloud point, the time when the first turbidity in the vessel can be visually detected, indicates that the nucleated particles have grown and agglomerated into a visually detectable range. Taking the cloud point as an indicator for the reaction time it can be seen that the mixing time in water is longer than the reaction time, whereas in sulphuric acid the mixing time is considerably shorter than the reaction time.

For a further description of the mixing in solution the specific energy input is needed which was found to be too small for an experimental determination. Even a build up torque measurement with a minimum power range of 0.1 W was not able to determine the energy input. However, from the torque measurement it could be taken that the total energy input into the system has to be smaller than 0.1 W. To estimate the lower limit of the energy input the measured mixing time was used. It can be assumed that the measured mixing time corresponds to the micro-mixing time, since for a complete color change the solution has to be mixed on the microscale. Since the degree of segregation is not known the energy input cannot be directly calculated from Eq. (3). For this purpose the specific energy input is calculated using Eq. (2) keeping in mind that the macro-mixing time is always shorter than the micro-mixing time thus getting the lower limit for the energy input. However, previously the Reynolds number ($Re = 2.2 \times 10^4$) was calculated using a stirrer diameter d of 0.04 m and a stirring speed n of 5 rpm to make sure that the condition of local isotropic turbulence is given. The dynamic viscosity and the density of the sulphate solution were taken to be equal to that of water at 80 °C with $\eta_{H_2O,80^\circ C} = 0.3544 \times 10^{-3}$ Pa s and $\rho_{H_2O,80^\circ C} = 971.82\ kg\ m^{-3}$ [39], respectively. Subsequently the macro-mixing time t_{macro} in dependence of the total energy input using Eq. (2) can be derived (Fig. 1).

For a macro-mixing time of 11 s a lower limit of about 1×10^{-4} W can be calculated which means that the size range of the energy input of the stirrer has to be between 1×10^{-4} W and 0.1 W. These limits of the energy input can then be used, given that the Schmidt number is much larger than one, to calculate the micro-mixing time. The Schmidt number was found to be about 3600 using a typical diffusion length of $1 \times 10^{-10}\ m^2\ s^{-1}$. Thus, the micro-mixing time for a degree of segregation of $I_s = 0.1$ (90% mixed) and $I_s = 0.01$ (99% mixed) can be derived (Fig. 2, Table 1).

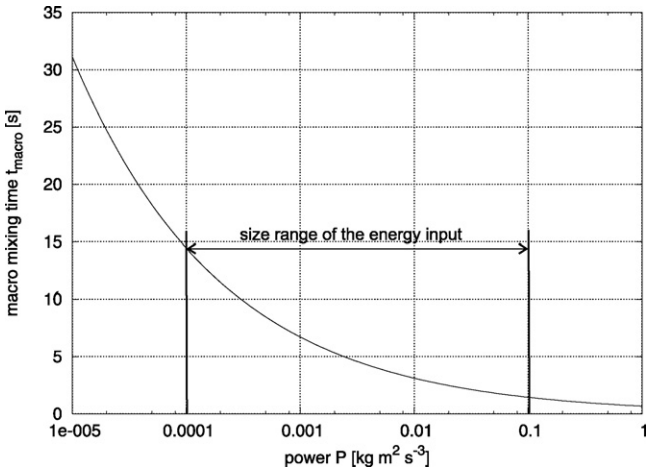

Fig. 1. Macro-mixing time in dependence of the total energy input.

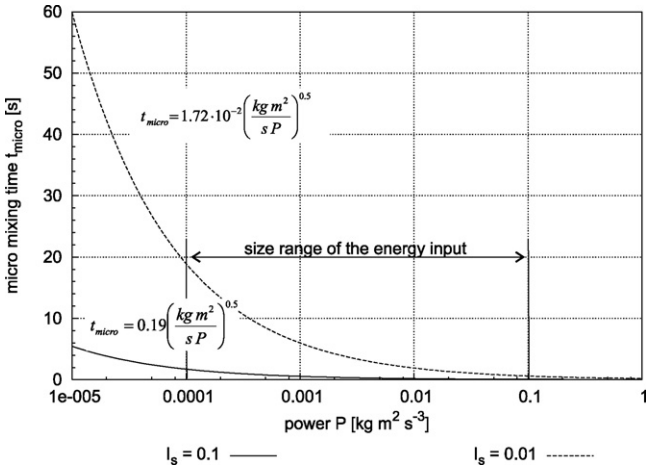

Fig. 2. Micro-mixing time in dependence of the power input for a degree of segregation of 0.1 and 0.01.

It can be seen that in 0.1 M H_2SO_4 the mixing time is considerably shorter than the reaction time so that for the theoretical description an ideally mixed system can be assumed.

In addition to the mixing time the Kolmogorov length scale was calculated to later on define the agglomeration mechanism. In Fig. 3 the Kolmogorov length scale in dependence of the power input is given.

The Kolmogorov length scale lies between 22 μm (0.1 W) and 124 μm (0.0001 W). As will be seen later the precipitated particles are smaller than about 25 μm showing that the particle agglomeration can be assumed to be based on Brownian motion which can be described by the perikinetic agglomeration kernel.

Table 1
Micro-mixing time in dependence of the total power input and the degree of segregation I_s.

Power input (W)	Degree of segregation	
	$I_s = 0.01$	$I_s = 0.1$
0.1	0.60 s	0.054 s
0.0001	18.9 s	1.72 s

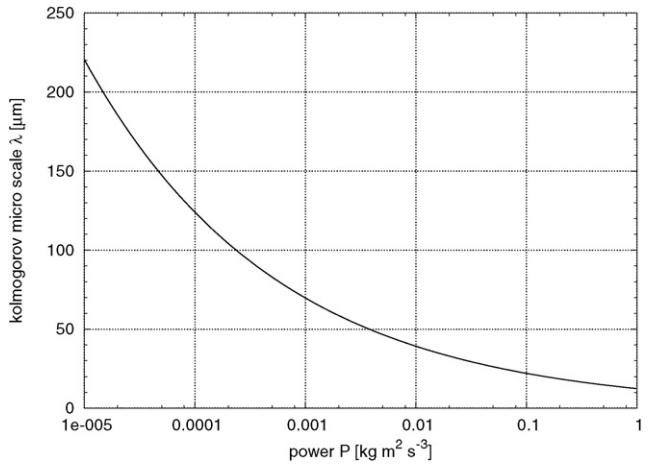

Fig. 3. Kolmogorov length scale in dependence of the power input.

4.2. Chemical hydrolysis in water and 0.1 M H_2SO_4

First of all the chemical kinetics in water and in diluted sulphuric acid were compared to each other to ascertain the influence of the additional sulphuric acid on the chemical reaction rate. For this purpose the reaction constants k_{r1} and k_{r2} with respect to a temperature of 80 °C for a 0.1 M $TiOSO_4{\cdot}H_2SO_4$ solution ($c(H_2SO_4)/c(TiOSO_4) = 1.15$) in water and 0.1 H_2SO_4 were calculated (table in Fig. 4) and the time-dependent formation of the precipitated TiO_2 compared to each other (Fig. 4). As can be seen the reaction constant k_{r1} in 0.1 M H_2SO_4 is only about half of the constant in water. Nevertheless, the influence on the formation of the precipitated material in the concentration range considered can practically be neglected. Furthermore, it can be seen that after about 50 s the chemical reaction has finished and all the material has been hydrolyzed. It is worth noting that the chemical reaction only represents the dissociation of the titanium oxysulphate and the hydrolyzation of the complex. These molecular precursors can then undergo olation and oxilation forming nuclei which can grow and agglomerate.

4.3. Precipitation rate in water and diluted sulphuric acid

4.3.1. Gravimetric analysis and UV/vis spectroscopy

As the second step the time-dependent precipitation of the material was investigated by the gravimetric analysis and UV/vis spectroscopy. In Fig. 5 the percentage of the precipitated TiO_2 measured by gravimetric analysis (left) and by UV/vis spectroscopy (right) for the different time steps and the two solutions are given.

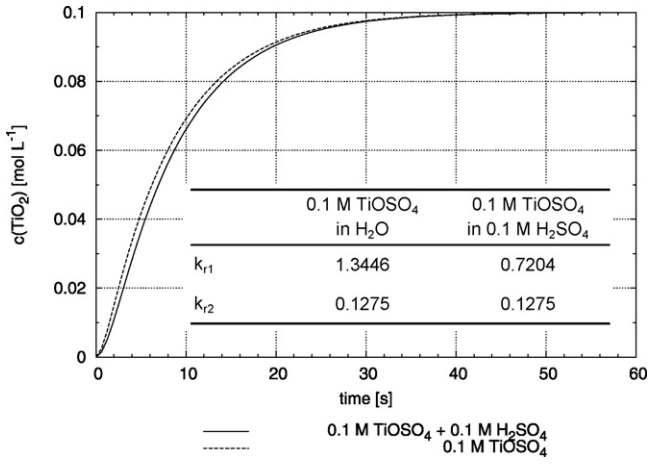

Fig. 4. Theoretical hydrolysis of a 0.1 $TiOSO_4$ solution in water and in 0.1 M H_2SO_4. In the table in the figure the reaction constants for both systems are given.

As can be seen in the gravimetric analysis the precipitation in water is faster than in sulphuric acid and additionally the total amount of precipitated material in water (90%) is much higher than in sulphuric acid (60%). This difference can already be seen in the beginning where in water after 1 min already 20% of the material is precipitated. This corresponds to the fact that the solution becomes turbid directly after the addition of the concentrated $TiOSO_4$. When the acidic solution is added to the solution with a pH of about seven there is a sharp rise of the pH which leads to a strong shift of the hydrolysis to the side of the product. Thus, the supersaturation, nucleation and agglomeration are strongly increased and particles can visually be detected. In diluted sulphuric acid there is not such a strong increase of the pH which prevents the shift of the equilibrium. However, in sulphuric acid only 60% of the material is precipitated, which leads to the question if the remaining material is present in the molecular state or in form of small particles which could not be held back by the filter. Therefore the experiments were repeated while the concentration of dissolved titanium dioxide was measured by UV/vis spectroscopy (Fig. 5, right). The UV/Vis measurement indicates that in water after 360 min almost 100% of TiO_2 is precipitated while in sulphuric acid about 85% is detected. This indicates that in water about 10% (0.4 g) and in sulphuric acid about 25% (1 g) of the material is present as small particles which cannot be held back by the filter and do not react with hydrogen peroxide. It cannot be explained up to now why in sulphuric acid still 15% of the titanium stays in solution after 6 h. To clarify this point additional spectroscopic measurements would be necessary.

4.3.2. Particle size measurement

The particle size distributions were measured after distinct time steps as described above and the volume weighted mean diameter $d_{4,3}$ (Fig. 6, top left) and the volume density distributions after 6 h (Fig. 6, top right) of the precipitation in water and in sulphuric acid were compared with each other. Additionally, SEM pictures after 6 h precipitation in water (Fig. 6, bottom left) and sulphuric acid (Fig. 6, bottom right) are shown.

It can be seen from the particle size distributions (PSD), the time-dependent mean particle diameter as well as from scanning electron microscopy pictures that the maximum mean particle size in sulphuric acid ($d_{4,3} \approx 23\,\mu m$) is higher than in water ($d_{4,3} \approx 15\,\mu m$). It is worth noticing that the mean particle diameter after about 50 min in water and 0.1 M sulphuric acid stays constant. It seems that there is a maximum agglomerate size, which means that the agglomeration stops after a certain size is reached although there is still an effective supersaturation.

It was shown that the hydrolysis of $TiOSO_4$ finishes within about 1 min whereas the final agglomerate size is reached after about 50 min. This indicates that during the precipitation the condensation or agglomeration are the rate determining steps while in comparison the time for hydrolyzation is quite small.

The PSD in sulphuric acid shows one peak between 10 and 50 μm while the distribution in water shows two distinct peaks, the first between 1 and 4 μm and the second between 5 and 35 μm. The smaller mean particle size in water can be explained by the fact that in the beginning due to the incomplete mixing and thus a high supersaturation a large number of nuclei are formed. These nuclei form agglomerates which can visually be detected directly after the addition. Although the supersaturation was decreased by the first outburst of nuclei, new particles are precipitated which can subsequently be gathered by the agglomerates present, leading to a relatively small distribution between 5 and 35 μm. However, it seems that a number of small particles (1–4 μm) are still present after 6 h. In sulphuric acid the nucleation is more a continuous

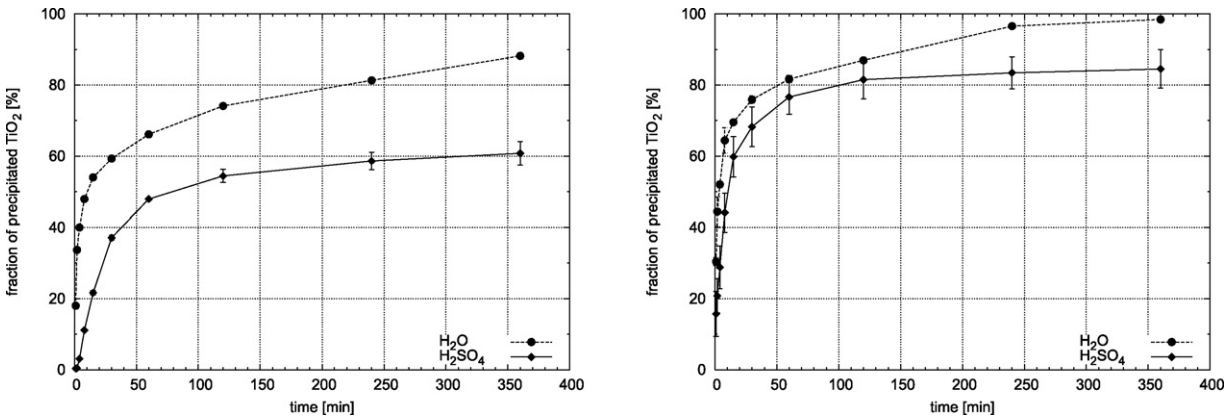

Fig. 5. Gravimetric analysis (left) and UV–vis measurement (right) of the precipitation in water and diluted sulphuric acid.

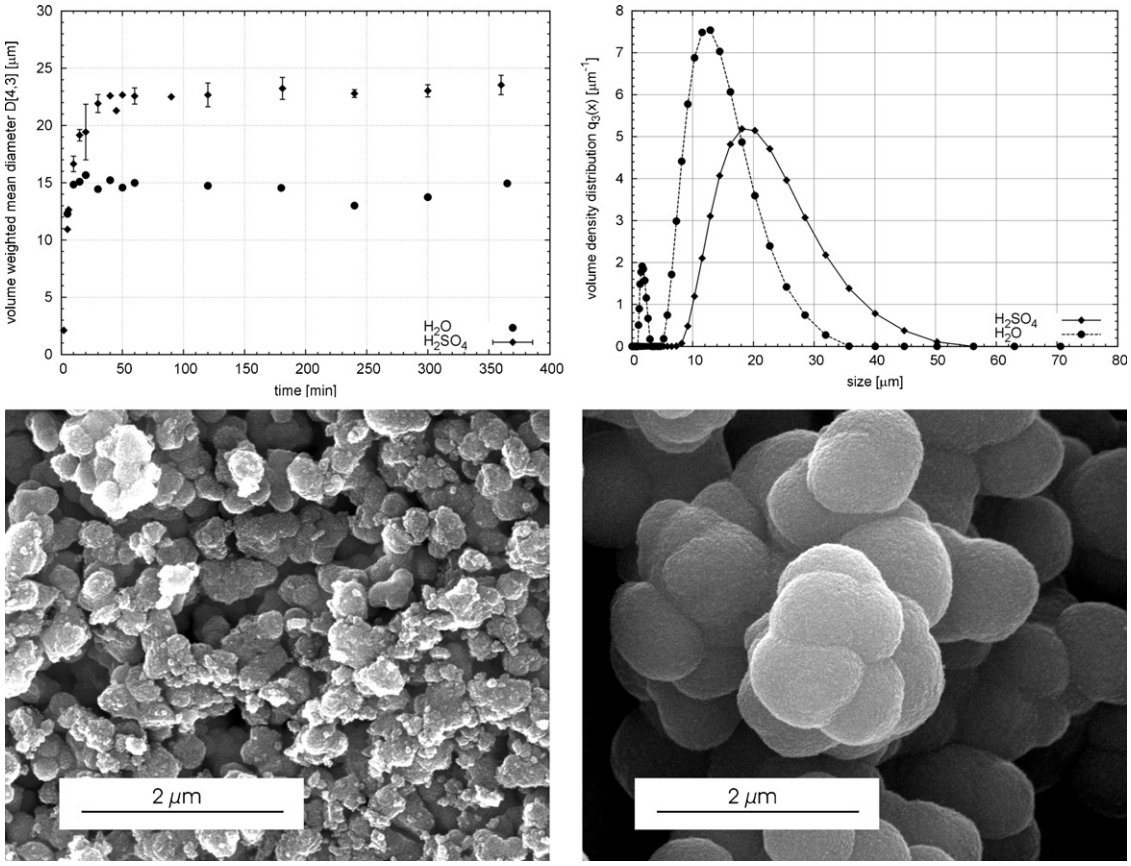

Fig. 6. Volume weighted mean diameter (top left), volume density distribution after 6 h (top right) and SEM pictures of particles precipitated in water (bottom left) and sulphuric acid (bottom right).

process. In the beginning the supersaturation stays at a high level since in nucleation only a small amount of material is consumed. Thus, for a longer time period particles are formed which can grow and undergo agglomeration forming a relatively broad distribution and larger particles. In contrast, it was found by X-ray diffraction that the primary particle sizes (Table 2) in water are larger than in sulphuric acid.

These dependencies are also in line with the previously given results of the precipitation of titanium dioxide. Due to the initial burst of particles in water and accordingly the decrease of supersaturation the growth of particles in this system plays a more dominant role than in sulphuric acid. Calculation of the number of primary particles from the mass of precipitated TiO_2 and the mean primary particle diameter after 4 h gives a total num-

Table 2
Primary particle sizes of the precipitation in water and sulphuric acid, measured by X-ray diffraction.

t (min)	Primary particle size (nm)	
	H_2O	H_2SO_4
15	2.7	0.8
30	3.5	1.1
60	4.3	2.2
240	4.9	3.2

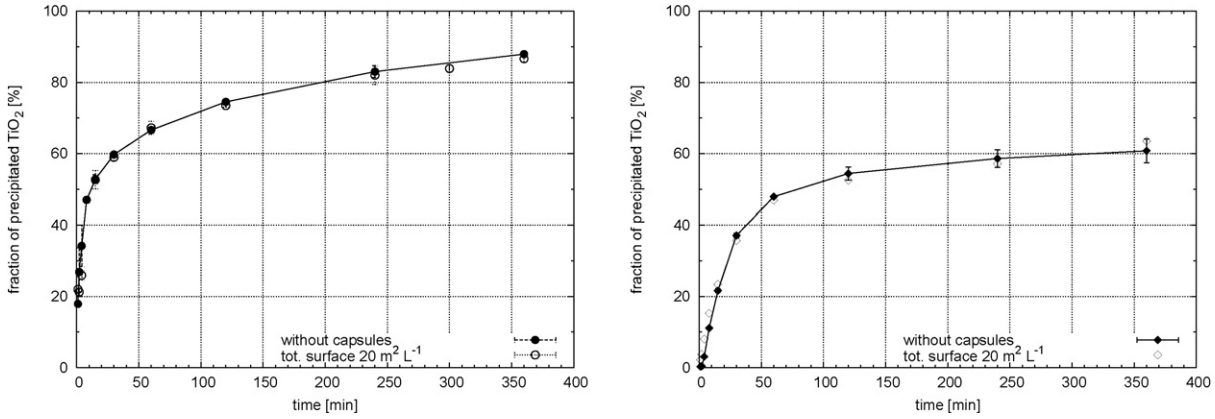

Fig. 7. Fraction of precipitated TiO_2 with and without capsules in water (left) and sulphuric acid (right).

ber of 1.65×10^{19} particles in water (d_{prim} = 4.9 nm, $m_{TiO_2} = 3.85$ g) and 5.02×10^{19} particles in sulphuric acid (d_{prim} = 3.2 nm, $m_{TiO_2} = 3.33$ g). This leads to the conclusion that in sulphuric acid more particles are formed which lead to larger agglomerates.

4.4. Coating of capsules

For the analysis of the coating process first of all the precipitation in the presence of capsules was investigated. Capsules were added to the reaction vessel and the experiment was performed as described above. It was found that in water (Fig. 7, left) and in sulphuric acid (Fig. 7, right) the addition of capsules does not have a significant influence on the precipitation rate. As can be seen the amount of precipitated mass in case of precipitation with and without capsules is practically the same. This clearly indicates that the nucleation is governed by homogeneous nucleation while heterogeneous nucleation can be neglected. This is reasonable taking into account the high supersaturation due to the low solubility of TiO_2 in water.

After determination of the overall precipitation in the system the coating rate of the capsules in sulphuric acid was investigated. In Fig. 8 (left) the weight percentage of TiO_2 precipitated on the capsules with respect to the mass of the coated capsules is shown. It can be seen that in case of the higher total surface area (20 m^2 L^{-1}) about 7 wt.% and in case of the smaller surface (4 m^2 L^{-1}) about 20 wt.% of the coated capsules consist of titanium dioxide. Due to the lack of heterogeneous nucleation on the surface of the capsules the coating rate is only dependent on the number of collisions between the template and the coating material. If the number of capsules represented by the total surface area is reduced the ratio of TiO_2 particles to capsules and accordingly the amount of precipitated material per capsule is increased.

In Fig. 8 (right) the rate of titanium dioxide which is part of the coating to the total amount of TiO_2 in the system is shown. As could be seen earlier the total amount of precipitated material (coating and in solution precipitated particles) is the same (60 wt.% after 6 h) with and without capsules. In the coating process in case of a total surface of 4 m^2 L^{-1} after 6 h about 20 wt.% of the overall precipitated material is part of the capsule coating while in case of a total surface of 20 m^2 L^{-1} about 30 wt.% of the precipitated material represents the capsule coating. Thus, with an increased template surface the yield of material precipitated on the template can be increased but in return the shell thickness for each template is reduced. This can only be overcome when an attractive potential between the template and the coating material can be established.

Another point which can be used for the control of the coating efficiency is the nucleation rate. In case of high nucleation rates a high number of TiO_2 particles are formed which can either agglomerate with capsules or with other oxide particles. The higher the number of TiO_2 particles the higher the probability of TiO_2–TiO_2 agglomeration compared to the agglomeration between capsules and TiO_2 particles. Thus, for an effective coating process low nucleation rates are favorable. This can for example be realized by higher concentrations of $TiOSO_4$ or H_2SO_4 or by the slow addition of a $TiOSO_4$ solution to a template dispersion.

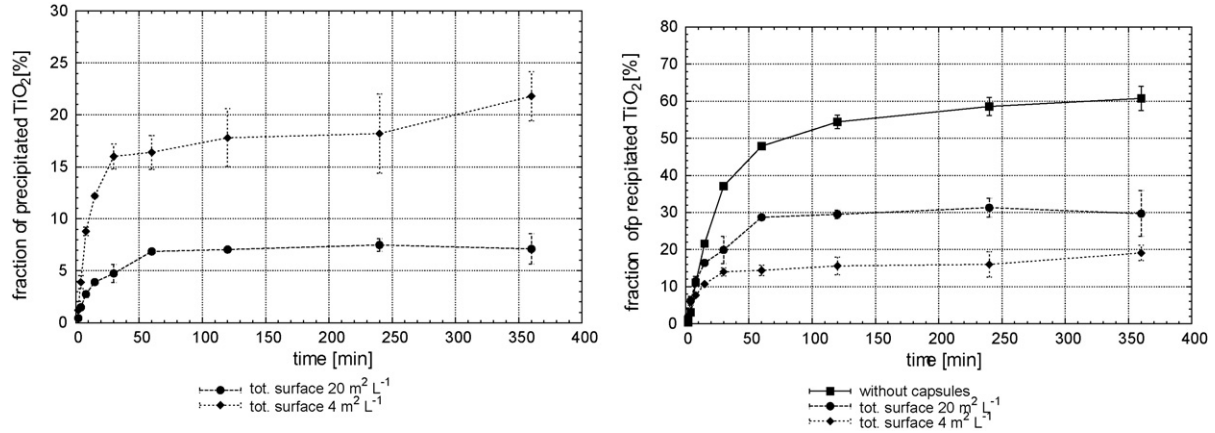

Fig. 8. Amount of precipitated titanium dioxide on the capsules with respect to the mass of the coated capsules (left) and with respect to the overall mass of TiO_2 in the system (right).

Table 3
Parameters of the equations used for the modeling of nucleation growth and agglomeration.

Process	Parameters	Fitted value	Equation
Nucleation	k_2	5.6×10^{48}	(7)
	k_3	3288	
Growth	$k_1 = k_g$	4×10^{-6}	(10)
	g	1.0	
Agglomeration	β_{br}	1×10^{-18}	(16)
	β_{tr}	0	

Furthermore, the agglomeration process can be influenced by careful control of the size of the template particles and the energy input into solution. As it was shown the agglomeration of the TiO_2 particles follows a perikinetic mechanism where agglomeration is only dependent on Brownian motion being independent of the stirrer speed. However, in case of core particles larger than the Kolmogorov microscale the velocity of the particles and thus the collision rate with the coating particles could be controlled by the energy input.

4.5. Modeling

Since it was found that the condition of an ideally mixed solution is only given for the precipitation in diluted sulphuric acid only this system was chosen for the modeling. For this system the chemical reaction rates k_{r1} and k_{r2} were taken as 0.7204 and 0.1275 mol L^{-1} s^{-1} (see Section 4.2), respectively. For the homogeneous precipitation the parameters for nucleation, growth and agglomeration given in Table 3 had to be fitted to the experimental data.

For a first approximation it can be assumed that only in nucleation and growth mass is consumed. Additionally, it can be stated that the volume based mean diameter $d_{4,3}$ is mainly affected by agglomeration, i.e. nucleation and growth can be neglected. Taking this into account the parameters for nucleation and growth were in parallel fitted to the precipitated mass while the agglomeration constants were fitted to the volume based mean diameter. Since 6 parameters had to be fitted manually it was only possible to find a local solution for the set while a global solution due to the high complexity of the system was not possible. However, the primary intention was not to find the very exact solution of the set of equations but to determine the influence of the individual parameters on the result of the modeling.

For a starting point for the theoretical description of nucleation and growth k_2 and k_3 were calculated using the classical theory of nucleation Eq. (6) with typical values. By this k_2 and k_3 were found to be about 5.6×10^{48} m^{-3} and 3288, respectively. Starting from this point the parameters k_2 and k_3 were fitted to the experimental data using the time-dependent precipitation measured by UV/vis spectroscopy. In a second step the agglomeration constant was fitted to the volume weighted mean diameter measured over time. Due to the fact that the agglomeration has an impact on the precipitation, since agglomeration reduces the overall surface of the particles which leads to a reduced precipitation by growth. By this, after tuning of the agglomeration constant, the nucleation and growth constants had to be refitted again. The fitting for the nucleation and growth as well as the agglomeration constants was repeated a number of times until the best correlation between the experiment and the theoretical results was reached. The parameters best fitting the experimental results are given in Table 3. In Fig. 9 the time-dependent precipitation (left) and volume weighted mean diameter (right) for this set of parameters together with the experimental data are shown.

It can be seen that the correlation between the model and the experimental data up to about 1200 s is quite good. After that time in the model the mass is continuously precipitated until the entire titanium dioxide is precipitated after about 2200 s. However, in the experiment it was found that the precipitated mass passes into a plateau at about 3.3 g although there is still a supersaturation of about 350. The nucleation constant with $k_2 = 1 \times 10^{48}$ m^{-3} is quite high, which was to be expected, since the equilibrium saturation of titanium dioxide is quite low and thus the supersaturation very high. The nucleation constant k_3 was taken as 3288, calculated from the classical theory of nucleation. It was found that there are different combinations of k_2 and k_3 which show very similar results. Due to the number of parameters and the high computational effort for the solution of one set of parameters it was not possible to determine if one of the other combinations would lead to a better fit.

After varying the parameters for nucleation and growth it was found that the precipitation in the initial time is dominated by nucleation which can be seen as a steep rise of the precipitated mass (grey shaded area in Fig. 9, left). A further increase of the nucleation constant would only lead to a higher amount of precipitated material in the initial time step and thus to a higher deviance between experiment and theory. In the subsequent time step it was found that the linear increase of the curve is clearly dominated by the growth term. In this part higher or lower growth rates lead to an increased or decreased slope, respectively.

Additionally, an increased growth term exponent, giving an idea about the growth mechanism, only leads to an increased slope with a higher deviance from the experimental data. Thus, a growth exponent of one seems to give the best fit to the experimental data

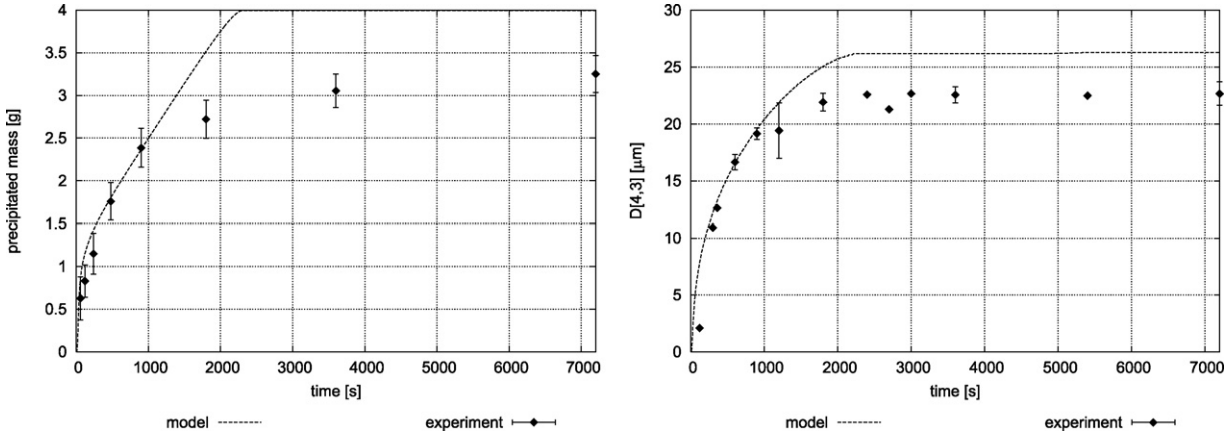

Fig. 9. Comparison of the model with the experimental data with respect to the time-dependent precipitation (left) and the volume weighted mean diameter (right).

which would lead to the assumption that the precipitation is best described by a diffusion controlled growth process. It can be seen that this simple model can be used to find the optimum parameters for nucleation, growth and agglomeration.

Comparing the theoretical and the experimental volume weighted mean diameter $d_{4,3}$ it can be seen that the correlation in the beginning is quite good. Up to about 1200 s the experimental data are exactly represented by the theoretical curve. After that the theoretical $d_{4,3}$ increases further until a mean diameter of about 27 μm is reached staying constant then. In this case the plateau can be explained by the fact that after about 2200 s the entire material is precipitated (see Fig. 9, left) preventing further agglomeration. If there were still supersaturation then the agglomeration would even proceed to larger mean particle sizes.

Comparing the results for the precipitation and the mean diameter, it can be seen that this simple model gives quite a good description of the process up to a time of about 1200 s. However, after that time the model deviates from the experimental curve giving an indication for a change in the precipitation mechanism that cannot be described using this simple model. However the model supports the finding that the process is based on Brownian motion.

5. Conclusion

In the present article it was shown that in the investigated system the precipitation in water is faster than in 0.1 M H_2SO_4. In water there is an initial outburst of particles due to the difference in pH between the concentrated $TiOSO_4$ solution and the water in the reaction vessel. By this difference locally very high reaction rates, faster than the mixing rate, are yielded. These fast reaction rates again lead to high local supersaturations followed by strong nucleation and agglomeration. Furthermore, the initially formed particles can collect the subsequent formed nuclei by agglomeration leading to a relative small particle size distribution, a small volume based mean particle diameter of about 15 μm and larger primary particle sizes than in sulphuric acid. In contrast in sulphuric acid the difference in pH is much smaller leading to a prolonged nucleation phase which leads to broader particle size distribution and a larger volume weighted mean diameter of about 23 μm. From the specific energy input into the system and the size of the capsules it can be deduced that in sulphuric acid the agglomeration is based on a perikinetic agglomeration mechanism.

In the coating process the precipitation rate is independent of the specific surface of the added capsules which shows that heterogeneous nucleation can be neglected in this process and that the coating efficiency only depends on the agglomeration between capsules and TiO_2. The latter can also be seen in the amount of TiO_2 on capsules in dependence of the capsule surface. With high specific surfaces of the capsules the amount of precipitated material which is part of the capsules increases while on the other hand the amount of titanium dioxide for each capsule decreases.

Conclusively it can be stated that for a high coating efficiency a slow nucleation rate (enough time for the capsules to collect the TiO_2 particles) and a large total surface area of the capsules are favorable.

The model used for the theoretical description process shows that the initial time step is governed by nucleation followed by a time step governed by growth. In addition, the model supports the experimental finding that the agglomeration is based on a perikinetic mechanism.

References

[1] A.F. Hollemann, E. Wiberg, Lehrbuch der anorganischen Chemie, 101st ed., Walter de Gruyter, Berlin, 1995, p. 1405.

[2] B.U. Grzmil, D.G. Grela, B. Kic, Studies on the hydrolysis process of titanium sulfate compounds, Chem. Pap. 62 (2007) 18–25.

[3] E. Santacesaria, M. Tonello, G. Storti, R.C. Pace, S. Carrat, Kinetics of titanium dioxide precipitation by thermal hydrolysis, J. Colloid Interface Sci. 111 (1986) 44–53.

[4] L.G. Gerasimova, R.F. Okhrimento, M.V. Maslova, Hydrolysis of Ti(IV) in the TiO_2–SiO_2–H_2SO_4–H_2O system during the preparation of a titanium silicate pigment, Theor. Found. Chem. Eng. 41 (2007) 620–622.

[5] H. Becker, E. Klein, H. Rechmann, Zum Wachstum von Titandioxydhydrat während der Hydrolyse von Titansulfatlösungen, Farbe und Lack 17 (1964) 779–787.

[6] S. Sathyamoorthy, G.D. Moggridge, M.J. Hounslow, Particle formation during anatase precipitation of seeded titanyl sulphate solution, Cryst. Growth Des. 1 (2001) 123–129.

[7] S. Sathyamoorthy, M.J. Hounslow, G.D. Moggridge, Influence of stirrer speed on the precipitation of anatase particles from titanyl sulphate solution, J. Cryst. Growth 223 (2001) 225–234.

[8] S. Sathyamoorthy, G.D. Moggridge, M.J. Hounslow, Controlling particle size during anatase precipitation, AIChE J. 47 (2001) 2012–2024.

[9] I.B. Jang, J.H. Sung, H.J. Choi, I. Chin, Synthesis and characterization of titania coated polystyrene core–shell spheres for electronic ink, Synth. Met. 152 (2005) 9–12.

[10] M. Sgraja, J. Bertling, R. Kümmel, P.J. Jansens, Inorganic and hybrid hollow spheres by coating of micropasules as templates, J. Mater. Sci. 41 (2006) 5490–5494.

[11] M. Sgraja, J. Blömer, J. Bertling, P.J. Jansens, In situ encapsulation of tetradecane droplets in oil-in-water emulsions using amino resins, J. Appl. Polym. Sci. 110 (2008) 2366–2373.

[12] B. Wielage, G. Leonhardt, Verbundwerkstoffe and Werkstoffverbunde, Wiley–VCH, Weinheim, 2001, pp.75–81.

[13] D.V. Bavykin, V.P. Dubovitskaya, A.V. Vorontsov, V.N. Parmon, Effect of $TiOSO_4$ hydrothermal hydrolysis conditions on TiO_2-morphology and gas-phase oxidative activity, Res. Chem. Intermed. 33 (2007) 449–464.

[14] J.-P. Jalava, E. Hiltunen, H. Kähkönen, H. Erkkilä, H. Härma, V.-M. Taavitsainen, Structural investigation of hydrous titanium dioxide precipitates and their formation by small-angle X-ray scattering, Ind. Eng. Chem. Res. 39 (2000) 349–361.

[15] W.P. Hsu, R. Yu, E. Matijevic, Paper whiteners—I. Titania coated silica, J. Colloid Interface Sci. 156 (1993) 56–65.

[16] P.A.A.P. Marques, T. Trindade, C.P. Neto, Titanium dioxide/cellulose nanocomposites prepared by a controlled hydrolysis method, Compos. Sci. Technol. 66 (2006) 1038–1044.

[17] M.C. Hidalgo, D. Bahnemann, Highly photoactive supported TiO_2 prepared by thermal hydrolysis of $TiOSO_4$: optimisation of the method and comparison with other synthetic routes, Appl. Catal. B 61 (2005) 259–266.

[18] D.V. Bavykin, E.N. Savinov, P.G. Smirniotis, A kinetics of the TiO_2 films growth at the hydrothermal hydrolysis of $TiOSO_4$, React. Kinet. Catal. Lett. 79 (2003) 77–84.

[19] A.N. Kolmogorov, Die lokale Struktur der Turbulenz in einer inkompressiblen zähen Flüssigkeit bei sehr großen Reynoldschen Zahlen, in: H. Goering (Ed.), Sammelband zur statistischen Theorie der Turbulenz, Academie Verlag, Berlin, 1958, pp. 71–76.

[20] R. Geisler, A. Mersmann, H. Voit, Makro- und Mikromischen im Rührkessel, Chem. Eng. Technol. 12 (1988) 947–955.

[21] A. Mersmann, H.D. Laufhütte, Scale-up agitated vessels for different mixing processes, in: 5th European Conference on Mixing, Würzburg, 1985, pp. 273–284.

[22] J.F. Duncan, R.G. Richards, Hydrolysis of titanium (IV) sulphate solutions—2. Solution equilibria, kinetics and mechanism, N. Z. J. Sci. 19 (1976) 179–183.

[23] J. Beukenkamp, K.D. Herrington, Ion-exchange investigation of the nature of titanium(IV) in sulfuric acid and perchloric acid, J. Am. Chem. Soc. 82 (1960) 3025–3031.

[24] A. Mersmann (Ed.), Crystallization Technology Handbook, 2nd edition, Marcel Dekker, New York, 2001.

[25] M. Kind, A. Mersmann, Methode zur Berechnung der homogenen Keimbildung aus wässrigen Lösungen, Chem. Eng. Technol. 55 (1983) 720–721.

[26] W. Stumm, J.J. Morgan, Aquatic Chemistry—Chemical Equilibria and Rates in Natural Waters, Wiley-Interscience, New York, 1996, p. 103.

[27] M.J. Hounslow, H.S. Mumtaz, A.P. Collier, J.P. Barrick, A.S. Bramley, A micromechanical model for the rate of aggregation during precipitation from solution, Chem. Eng. Sci. 56 (2001) 2543–2552.

[28] M.v. Smoluchowski, Versuch einer mathematischen Theorie der Koagualtionskinetik kolloider Lösungen, Z. Phys. Chem. 92 (1916) 129–168.

[29] A.D. Randolph, M.A. Larson, Theory of Particulate Processes, 2nd ed., Academic Press, San Diego, 1988, p. 187.

[30] K. Zafar, Solution of the Population Balance Equations for the Micro-particle Coating, Master Thesis, Fraunhofer Institut Umwelt-, Sicherheits-, Energietechnik UMSICHT, 2004, p. 10.

[31] P.W. Atkins, Physical Chemistry, 5th ed., Oxford University Press, Oxford, 1994, p. 884.

[32] Y.I. Lim, J.-M. Le Lann, X.M. Meyer, X. Joulia, G. Lee, E.S. Yoon, On the solution of population balance equations (PBE) with accurate front tracking methods in practical crystallization processes, Chem. Eng. Sci. 57 (2002) 3715–3732.

[33] G.-S. Jiang, C.-W. Shu, Efficient implementation of weighted ENO schemes, J. Comput. Phys. 126 (1996) 202–228.

[34] H. Yang, An artificial compression method for ENO schemes, the slope modification method, J. Comput. Phys. 89 (1990) 125–160.

[35] S. Kumar, D. Ramkrishna, On the solution of population balance equations by discretization—I. A fixed pivot technique, Chem. Eng. Sci. 51 (1996) 1311–1332.
[36] E. Riedel (Ed.), Anorganische Chemie, Walter de Gruyter, Berlin, 1989, p. 690.
[38] C. Hammond, The Basis of Crystallography and Diffraction, IUCr Texts on Crystallography 3, Oxford Science Publications, Oxford, 1997, p. 146.
[39] D.R. Lide, H.P.R. Frederikse (Eds.), Handbook of Chemistry and Physics, 78th ed., CRC Press, New York, 1997, p. 6-3.